^{13}N-Ammonia PET/CT Detection of Myocardial Perfusion Abnormalities in Beagle Dogs After Local Heart Irradiation

Jianbo Song[1,2], Rui Yan[1,3], Zhifang Wu[1], Jianguo Li[4], Min Yan[1], Xinzhong Hao[1], Jianzhong Liu[1], and Sijin Li[1]

[1]Department of Nuclear Medicine, First Hospital of Shanxi Medical University, Shanxi, China; [2]Department of Radiotherapy, Shanxi Academy of Medical Sciences, Affiliated Shanxi Dayi Hospital of Shanxi Medical University, Shanxi, China; [3]Nursing College, Shanxi Medical University, Shanxi, China; and [4]Department of Radiological and Environmental Medicine, China Institute for Radiation Protection, Shanxi, China

Our objective was to determine the potential value of ^{13}N-ammonia PET/CT myocardial perfusion imaging (MPI) for early detection of myocardial perfusion changes induced by radiation damage. **Methods:** Thirty-six Beagle dogs were randomly divided into a control group (n = 18) or an irradiation group (n = 18). The latter underwent local irradiation to the left ventricular anterior cardiac wall with a single dose of 20 Gy, whereas the former received sham irradiation. All dogs underwent ^{13}N-ammonia PET/CT MPI 1 wk before irradiation and at 3, 6, and 12 mo after sham or local irradiation. One week after undergoing ^{13}N-ammonia PET/CT MPI, the irradiation group underwent coronary angiography. Six randomly selected dogs from each group were sacrificed and used to detect pathologic cardiac injury at 3, 6, and 12 mo after irradiation. **Results:** Compared with the control group and baseline, the irradiation group showed significantly increased perfusion in the irradiated area of the heart at 3 mo after irradiation, perfusion reduction at 6 mo after irradiation, and a perfusion defect at 12 mo after irradiation. There was no significant difference in the left ventricular ejection fraction between the control and irradiation groups at baseline or at 3 mo after irradiation. The irradiation group showed a reduction of left ventricular ejection fraction compared with the control group at 6 mo (50.0% ± 8.1% vs. 59.3% ± 4.1%, P = 0.016) and 12 mo (47.2% ± 6.7% vs. 57.4% ± 3.3%, P = 0.002) after irradiation. No coronary stenosis was observed in the irradiation group. Regional wall motion abnormalities appeared in the irradiated area at 6 mo after irradiation, and its extent was enlarged at 12 mo after irradiation. Pathologic changes were observed; radiation-induced myocardial tissue damage and microvascular fibrosis in the irradiated area progressively increased over time. **Conclusion:** ^{13}N-ammonia PET/CT MPI can dynamically detect myocardial perfusion changes together with global and regional left ventricular dysfunction induced by irradiation and may be a valuable method for monitoring radiation-induced heart disease.

Key Words: radiotherapy; radiation-induced heart disease; myocardial perfusion imaging; ^{13}N-ammonia PET/CT

J Nucl Med 2017; 58:605–610
DOI: 10.2967/jnumed.116.179697

Radiotherapy is an effective treatment for many chest tumors, including breast cancer, lung cancer, esophageal cancer, Hodgkin lymphoma, and so on. Several studies have demonstrated that radiation-induced heart disease (RIHD) increases in a dose-dependent manner in patients who undergo thoracic radiotherapy. Among these patients, RIHD is the most common noncancer cause of death. The survival benefit obtained from radiotherapy can be counteracted by an increased risk of RIHD (*1–3*). Today, the heart is considered a key organ at risk from radiotherapy. With the development of sophisticated radiotherapy techniques such as intensity-modulated radiation therapy, image-guided radiation therapy, and TomoTherapy (Accuray), radiation oncologists are able to deliver doses with far greater accuracy than previously, significantly reducing the radiation dose to cardiac tissue. However, most thoracic radiotherapy patients still receive either a high dose of radiation to a small part of the heart or a lower dose to the whole heart (*4–7*). There is no minimum threshold dose below which radiation is considered safe. Even lower doses can increase the morbidity and the mortality of heart diseases (*8–11*). Because of the lack of convincing proof from multicenter trials with a sufficient follow-up period, the true incidence of RIHD is uncertain (*4,12*). Early diagnosis of RIHD can facilitate timely interventions and may improve the prognosis of these patients. However, there are currently no accepted guidelines for RIHD screening and surveillance (*13–15*). Therefore, the objective of this study was to investigate perfusion changes and pathologic changes in Beagle dogs with RIHD using ^{13}N-ammonia PET/CT myocardial perfusion imaging (MPI) and to determine the feasibility of monitoring RIHD by this method.

MATERIALS AND METHODS

Animals

In this study, all animal care and experimental procedures complied with the guidebook of the Institutional Animal Care and Use Committee. Thirty-six male 12-mo-old Beagle dogs (mean weight ± SD, 12 ± 0.67 kg) were purchased from the Anhui Fuyang Weiguang Institute of Experimental Animals. After approximately 1 wk of quarantine, the dogs were randomly assigned to a control group or an irradiation group, which received local heart irradiation. All animals were housed individually at the Experimental Animal Center of the China Institute for Radiation Protection in stainless steel cages in an air-conditioned facility (18°C–25°C; relative humidity, 40%–60%; ≥12 air changes/h) and fed standard certified commercial dog chow twice daily, with water available ad libitum. Before the study, the

Received Jul. 13, 2016; revision accepted Nov. 25, 2016.
For correspondence or reprints contact: Sijin Li, Department of Nuclear Medicine, First Hospital of Shanxi Medical University, No. 85, Jiefang Rd., Taiyuan, Shanxi 030001, China.
E-mail: lisj_nm1@sohu.com
Published online Dec. 1, 2016.
COPYRIGHT © 2017 by the Society of Nuclear Medicine and Molecular Imaging.

dogs were acclimated to these conditions for 2 wk. All animals underwent ^{13}N-ammonia MPI, and those in the irradiation group underwent coronary angiography before local irradiation and at 3, 6, and 12 mo afterward. Six animals randomly selected from each group were sacrificed at each time point, and their hearts were taken for pathologic testing. The study was approved by our Institutional Animal Care and Use Committee and was performed in accordance with the Guidelines for Animal Experiments of Shanxi Medical University.

Local Heart Irradiation

The animals were anesthetized by intravenous injection with 3% pentobarbital sodium at 30 mg/kg and fixed supine by a vacuum-form body immobilizer. All underwent a control enhanced CT simulation scan (Discovery VCT64 PET/CT scanner; GE Healthcare) for radiotherapy planning. After scanning, the images were transmitted to an Eclipse TPS system (Varian). The anterior wall of the left ventricle was outlined as the radiation target, accounting for one quarter to one third of the left ventricular volume, and a conformal intensity-modulated radiation therapy plan was made. Cone-beam CT was performed with a flat-panel detector to verify the accuracy of the target location before exposure. After location verification, the dogs in the irradiation group received a single 20-Gy dose of irradiation with 6-MV x-rays, and the dogs in the control group underwent the same procedure but without the irradiation.

^{13}N-Ammonia MPI

After 12 h of fasting, the dogs were anesthetized, fixed supine, transferred to the bed of the PET/CT scanner (Discovery VCT; GE Healthcare), and connected to the electrocardiogram monitor. First, a CT scout scan was acquired to locate the position of the heart in the scanner field of view, using 120 kVp, 30–50 mA, and a slice thickness of 3.75 mm. Next, 148–185 MBq (4–5 mCi) of ^{13}N-ammonia were administered by an intravenous bolus, and the PET scan was performed 3 min afterward. PET data were acquired in 3-dimensional mode for 10 min. Images were reconstructed using the iterative method, with a matrix of 128 × 128 pixels, 2 iterations, and 6 subsets, and corrected for attenuation using attenuation data from the CT component of the examination.

Image Analysis

Images were processed using Myovation software in a Xeleris 4.3 workstation (GE Healthcare). PET/CT images were independently reviewed by *2* experienced nuclear medicine physicians in a double-masked fashion; 2 observers analyzed all images from every subject slice by slice. In the semiquantitative analysis, a same-sized region of interest in both the anterior wall (irradiated area) and the posterior wall (nonirradiated area) was delineated at 3 different levels of the ventricle on the PET/CT images, and the average radioactivity count was used to calculate the irradiation-to-nonirradiation activity ratio. Gated studies were quantitatively analyzed using quantitative gated SPECT software; the parameters regional wall motion, end-diastolic volume, end-systolic volume, and left ventricular ejection fraction were acquired automatically; and the polar bull's-eye plot was divided into 20 segments.

Coronary Angiography

One week after undergoing ^{13}N-ammonia myocardial perfusion PET/CT, the irradiation group underwent coronary angiography. In the catheterization laboratory, the anesthetized dogs were placed supine after bilateral preparation of the inguinal skin. Using a Judkin catheter, a cardiologist conducted the coronary angiography procedure. Two experienced interventional cardiologists assessed the results using the Thrombolysis in Myocardial Infarction score (*16*), which categorizes coronary blood flow as grade 0 (no perfusion), 1 (penetration without perfusion), 2 (partial perfusion), or 3 (complete perfusion).

Histologic Assessment

The dogs were euthanized under anesthesia by acute blood loss; the ribs were cut along the left sternal border, the thoracic cavity was exposed, and the heart was quickly removed. The atrial tissue was then removed from the heart, and the ventricular tissue was prepared for histologic evaluation by immersion and fixation in 10% formalin. For each heart, myocardial tissue was taken from the anterior wall (irradiated area) and the posterior wall (nonirradiated area) at the middle level of the left ventricle. All tissue samples were fixed, trimmed, washed, and progressively dehydrated in ethanol. The alcohol was then replaced with xylene, and the samples were embedded in a paraffin block. From each block, 5-μm-thick sections were prepared and stained with hematoxylin–eosin, CD31 immunostain, and Masson trichrome stain. Morphologic changes were observed by light microscopy (JEM-2100; JEOL Co.). Myocardial degeneration and vascular injury were measured semiquantitatively to evaluate the extent of cardiac damage (*17,18*).

To evaluate myocardial degeneration, 6 nonvascular microscopic fields (×200) were randomly selected from the hematoxylin- and eosin-stained slices and graded as 0 (normal: no degeneration of myocardial cells), 1 (mild: <20% degeneration of myocardial cells), 2 (moderate: ~20%–50% degeneration of myocardial cells), or 3 (severe: >50% degeneration of myocardial cells).

To evaluate myocardial vascular injury, 6 vascular microscopic fields (×200) were randomly selected from the hematoxylin- and eosin-stained slices and graded as 0 (no fibrosis: adventitia thickness ≈ half the media), 1 (mild fibrosis: adventitia thickness ≈ the media), 2 (moderate fibrosis: adventitia thickness ≈ 2 × the media), or 3 (severe fibrosis: adventitia thickness ≥ 3 × the media).

To evaluate myocardial microvessel density, 6 independent microscopic fields (×200) were randomly selected from the CD31-immunostained slices. The percentage of blood vessels involved per visual field was graded as 0 (absent), 1 (<10%), 2 (10%–50%), or 3 (>50%) (*19*).

To evaluate cardiac interstitial fibrosis, 6 independent microscopic fields (×200) were randomly selected from the Masson-stained slices and graded as 0 (no apparent collagen fiber proliferation), 1 (focal and minimal fibrosis), 2 (mild patchy fibrosis), 3 (moderate diffuse fibrosis), or 4 (most prominent fibrosis) (*20*).

Statistical Analysis

All quantitative data were expressed as mean ± SD. Differences between groups were tested using a *t* test and ANOVA and using a rank sum test for ordinal data. Statistical significance was accepted at a P level of less than 0.05. The SPSS 18.0 software package (IBM) was used for statistical analyses.

RESULTS

Animal Conditions

One week before irradiation and at 3, 6, and 12 mo after irradiation, the average weights of the animals in the irradiation group were 11.0 ± 1.0 kg, 13.0 ± 0.7 kg, 14.0 ± 1.0 kg, and 15.0 ± 0.7 kg, respectively. At the same time points, the average weights of the animals in the control group were 12.0 ± 0.1 kg, 13.0 ± 0.8 kg, 15.0 ± 0.1 kg, and 15.0 ± 0.8 kg, respectively. There were no significant differences in diet, weight, heart rate, blood pressure, or mental status between the two groups. No symptoms of heart failure were observed after irradiation.

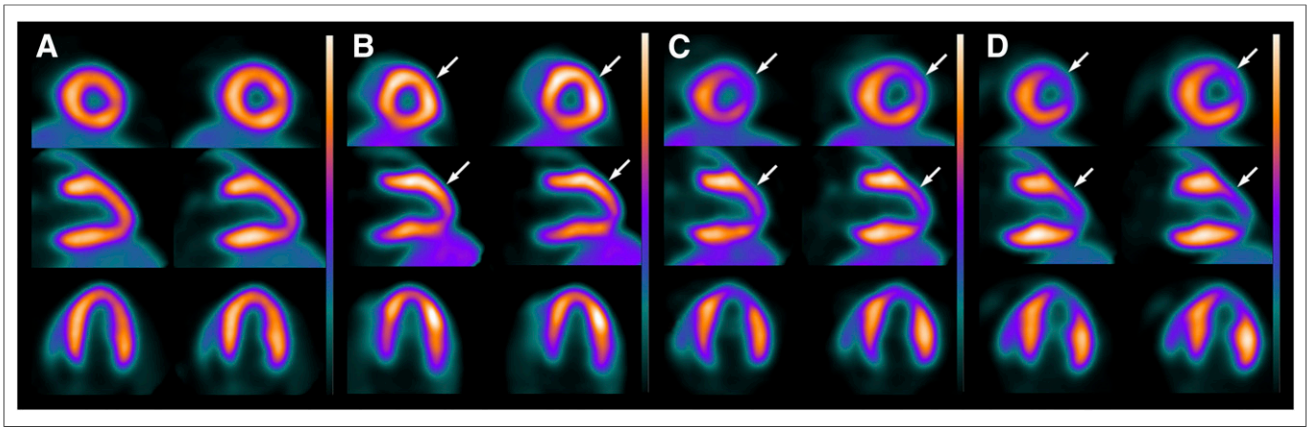

FIGURE 1. ^{13}N-ammonia MPI before radiation and 3, 6, and 12 mo after irradiation. (A–C) Myocardial perfusion is normal before irradiation (A), increased at 3 mo after irradiation (arrow, B), and reduced at 6 mo after irradiation (arrow, C). (D) A perfusion defect is seen at 12 mo after irradiation (arrow).

^{13}N-Ammonia PET/CT MPI

Compared with the control group and baseline, the irradiation group showed increased perfusion in the irradiated area of the heart at 3 mo after irradiation; a reduction in perfusion was seen at 6 mo after irradiation, and perfusion defects were seen at 12 mo after irradiation (Figs. 1 and 2).

Irradiation-to-Nonirradiation Activity Ratio

There were no significant differences in the irradiation-to-nonirradiation activity ratio between the control and irradiation groups before irradiation. Compared with the control group, the irradiation group had an increased ratio at 3 mo after irradiation (1.2 ± 0.1 vs. 1.0 ± 0.1, $P < 0.05$), a decreased ratio at 6 mo after irradiation (0.9 ± 0.3 vs. 1.0 ± 0.9, $P < 0.05$), and a significantly decreased ratio at 12 mo after irradiation (0.7 ± 0.4 vs. 1.0 ± 0.3, $P < 0.01$) (Table 1).

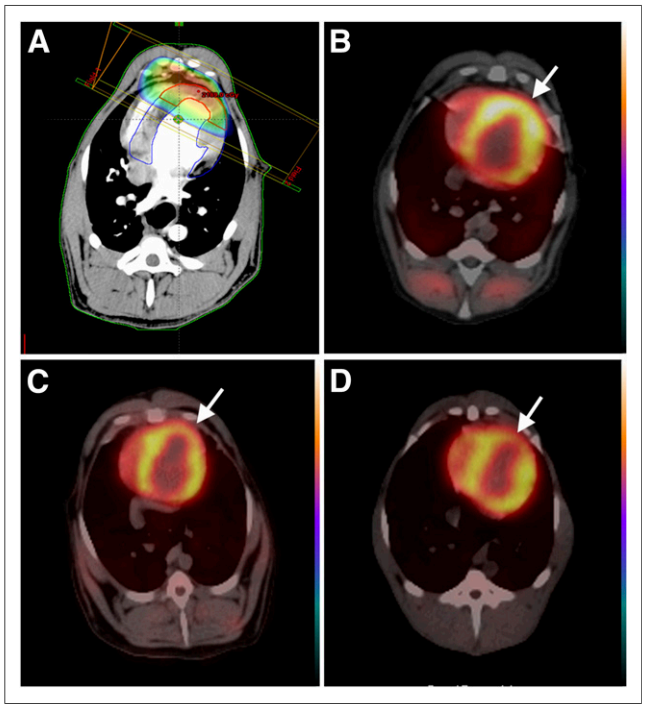

FIGURE 2. (A) Radiation field and radiation dose distribution. (B–D) PET/CT fusion images showing that scope of perfusion abnormality is consistent with radiation field at 3 mo (B), 6 mo (C), and 12 mo (D) after irradiation (arrows).

Left Ventricular Function

No statistically significant differences were observed between the irradiation group and the control group in end-diastolic volume, end-systolic volume, or left ventricular ejection fraction before irradiation and at 3 mo after irradiation. Similarly, there was no difference in end-diastolic volume at 6 mo after irradiation; however, end-systolic volume was significantly higher (13.4 ± 2.2 mL vs. 10.3 ± 1.7 mL, $P < 0.05$)—and left ventricular ejection fraction significantly lower ($50.0\% \pm 8.1\%$ vs. $59.3\% \pm 4.1\%$, $P < 0.05$)—in the irradiation group than in the control group. Interestingly, at 12 mo after irradiation, both end-diastolic volume (26.5 ± 2.5 mL vs. 22.8 ± 3.2 mL, $P < 0.05$) and end-systolic volume (14.1 ± 2.0 mL vs. 10.4 ± 2.1 mL, $P < 0.01$) were significantly larger in the irradiation group than in the control group, and left ventricular ejection fraction ($47.2\% \pm 6.7\%$ vs. $57.4\% \pm 3.3\%$, $P < 0.01$) was significantly lower (Table 2). No obvious abnormal ventricular wall motion was observed in either of the two groups at 3 mo after irradiation. Regional ventricular wall-motion abnormalities were commonly observed in or adjacent to the irradiation area, with 5 segments involved at 6 mo after irradiation and 11 segments at 12 mo (Supplemental Table 1; supplemental materials are available at http://jnm.snmjournals.org).

TABLE 1
Comparison of Irradiation-to-Nonirradiation Activity Ratio Between Control and Irradiation Groups

Group	Before irradiation	Time after irradiation		
		3 mo	6 mo	12 mo
Control	1.0 ± 0.1	1.0 ± 0.1	1.0 ± 0.9	1.0 ± 0.3
Irradiation	1.1 ± 0.2	1.2 ± 0.1	0.9 ± 0.3	0.7 ± 0.4
P	0.9	0.047	0.015	<0.01

TABLE 2
Comparison of Functional Parameters of Left Ventricle Between Control and Irradiation Groups

Parameter	Before irradiation	Time after irradiation		
		3 mo	6 mo	12 mo
Left ventricular ejection fraction (%)				
Control group	59.6 ± 5.2	58.9 ± 3.0	59.3 ± 4.1	57.4 ± 3.3
Irradiation group	58.9 ± 5.6	56.4 ± 4.0	50.0 ± 8.1	47.2 ± 6.7
P	0.808	0.227	0.016	0.002
End-diastolic volume (mL)				
Control group	23.4 ± 2.8	23.4 ± 2.2	24.3 ± 2.3	22.8 ± 3.2
Irradiation group	23.6 ± 2.6	23.9 ± 4.2	23.3 ± 3.6	26.5 ± 2.5
P	0.923	0.816	0.952	0.014
End-systolic volume (mL)				
Control group	11.1 ± 2.1	11.2 ± 1.5	10.3 ± 1.7	10.4 ± 2.1
Irradiation group	10.4 ± 2.0	10.6 ± 4.7	13.4 ± 2.2	14.1 ± 2.0
P	0.490	0.491	0.01	0.001

Coronary Angiography

No coronary stenosis was observed in the irradiation group at baseline or at 3, 6, or 12 mo after irradiation. All irradiation groups had grade 3 coronary flow according to the designation of the Thrombolysis in Myocardial Infarction trial (Fig. 3).

Histologic Results

In the control group, the myocardial tissue was normal; no significant changes from baseline were observed at 3, 6, or 12 mo after irradiation (Fig. 4A). Compared with the control group and the nonirradiated area, the irradiated area showed slightly increased myocardial interstitial fibrosis at 3 mo after irradiation and a small degree of fibrous tissue hyperplasia, interstitial small-vessel wall thickening, and perivascular fibrosis (Fig. 4B; Table 3). Six months after irradiation, some areas of the left ventricle showed myocardial degeneration, moderate myocardial interstitial fibrosis, and obvious interstitial small-vessel wall thickening but no myocardial necrosis (Fig. 4C; Table 3). Twelve months after irradiation, the myocardial tissue had severe damage, with significant myocardial tissue degeneration and myocardial interstitial fibrosis, interstitial vessel wall thickening, and perivascular fibrosis (Fig. 4D; Table 3). There was no obvious inflammatory cell infiltration in the irradiated area. Masson staining showed that myocardial interstitial fibrosis increased progressively after irradiation (Supplemental Fig. 1). CD31 immunostaining showed that myocardial interstitial microvessel density was significantly increased in the irradiated area at 3 mo after irradiation (Supplemental Fig. 2B). With the progression of radiation-induced myocardial tissue damage, the density of interstitial microvessels in the myocardium gradually decreased by 6 and 12 mo after irradiation (Supplemental Figs. 2C and 2D). In the nonirradiated area, hematoxylin–eosin and Masson staining showed no significant abnormalities in the myocardial tissue, and CD31 immunostaining showed a slight compensatory increase in microvessel density at 3, 6, and 12 mo after irradiation.

DISCUSSION

With the progress in radiotherapy technology, the disease-specific and overall survival rates of cancer patients have improved significantly. The issue of toxicity in thoracic radiation patients has been gaining attention, and the existence of RIHD has been confirmed by studies on animals and cancer patients. Moreover, RIHD is often subclinical and may not manifest until years after radiotherapy. Its exact prevalence is unclear and, likely, has been underreported. The available evidence indicates that multidisciplinary follow-up and screening for RIHD is necessary (*13,14,21*). Early diagnosis of RIHD can promote timely clinical interventions and may improve the prognosis, but the ideal screening method and frequency remain unclear, and the mechanisms of injury in RIHD remain largely unknown (*22*).

Marks et al. (*23,24*) conducted a prospective study to evaluate the changes in myocardial perfusion and cardiac function in irradiated patients for left-sided breast cancer, and a 50%–63% incidence of new perfusion defects was observed. Gayed et al. (*25,26*) often observed myocardial perfusion abnormalities in a SPECT MPI follow-up study on a small group of esophageal and lung cancer patients after radiotherapy. Furthermore, patients with perfusion defects are often clinically asymptomatic, and the long-term clinical significance of these perfusion abnormalities remains uncertain (*13,27,28*). In this study, we applied a single 20-Gy dose of local irradiation to the anterior myocardial wall in Beagle dogs, simulating clinical high-dose radiation for local

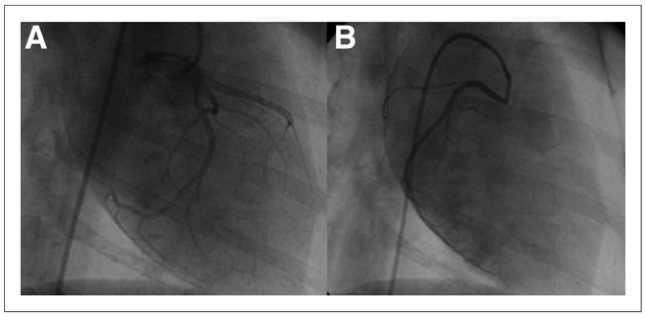

FIGURE 3. Coronary angiography in irradiation group showing no stenosis at 12 mo after irradiation in left coronary artery (A) or right coronary artery (B).

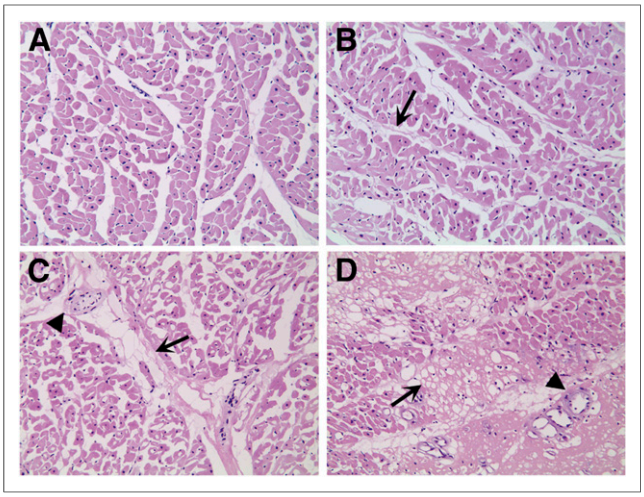

FIGURE 4. Hematoxylin–eosin staining of myocardium in control group (A) and at 3 mo (B), 6 mo (C), and 12 mo (D) after irradiation (magnification, ×200). At 3 mo after irradiation, mild myocardial cell deformation and interstitial fiber hyperplasia were observed (arrow). At 6 mo after irradiation, obvious myocardial tissue degeneration, moderate myocardial interstitial fibrosis (arrow), and vessel wall thickening were observed (arrowhead). At 12 mo after irradiation, patchy myocardial necrosis and diffuse interstitial fibrosis (arrow), significant vessel wall thickening, and perivascular fibrosis were observed (arrowhead).

cardiac tissue and allowing comparison of the irradiated and nonirradiated areas. At the same time, we monitored the changes in myocardial blood flow in both the irradiated and nonirradiated areas using ^{13}N-ammonia PET/CT MPI. In contrast to clinical investigations, animal experiments can eliminate the effects of irradiation position, dose or volume differences, the inclusion criteria of chemotherapy, the conventional high risks of heart disease, and other confounding factors.

In contrast to previous reports (*23–26*), we found that at 3 mo after irradiation, perfusion was increased in the irradiated field compared with the nonirradiated field and the control field, and no functional changes were observed in the heart. These differences may have been due to scanning at different time points after radiation in different studies or because ^{13}N-ammonia PET/CT MPI has higher sensitivity and specificity than SPECT MPI in quantifying myocardial perfusion. The myocardial pathologic examination showed a small amount of myocardial cell degeneration, microvascular dilation, microvessel density increase, and capillary wall thickening in the irradiated tissue; these injuries may have increased capillary permeability, resulting in increased perfusion flow. Six months after irradiation, the irradiated areas showed decreased perfusion, and cardiac function and left ventricular ejection fraction were decreased. In clinical research, Gyenes et al. (*29*) and Seddon et al. (*30*) also often observed reduced regional myocardial perfusion in patients with left-sided breast cancer at 6 mo or more after radiotherapy. Pathologic examination at the same time point identified mild myocardial degeneration, microvascular wall fibrosis and stenosis, and interstitial fibrosis. Twelve months after irradiation, the irradiated areas exhibited myocardial perfusion defects, and left ventricular function was further reduced. In terms of concomitant pathology, we found that radiation-related myocardial damage was further aggravated by visible myocardial degeneration and a small area of myocardial necrosis, microvascular wall fibrosis, microvascular luminal stenosis and occlusion, and significantly increased interstitial fibrosis. The irradiation-to-nonirradiation activity ratio, which may be more accurate than visual observation in reflecting myocardial perfusion changes in the irradiation area and is less affected by the other factors, may be a more sensitive indicator for monitoring RIHD. A progressive increase in microvascular damage, myocardial degeneration, and interstitial fibrosis may together result in the decreased myocardial perfusion flow and regional left ventricular wall motion abnormalities at 6 and 12 mo after irradiation. In general, myocardial fibrosis is a major endpoint for RIHD, and microvascular damage and myocardial degeneration may aggravate myocardial fibrosis; further work evaluating the exact biochemical mechanisms of RIHD is warranted.

From 3 to 12 mo after irradiation, MPI perfusion abnormalities correlated spatially to the 3-dimensional myocardial dose distribution computed with the CT dataset, whereas coronary angiography found no abnormalities. These results suggest that perfusion abnormalities caused by radiation-induced injury to the myocardial microvasculature are generally limited to the radiation field and do not correspond to the distribution of the coronary vessels.

TABLE 3
Comparison of Histologic Parameters Between Control and Irradiation Groups

	Myocardial degeneration						Myocardial vascular injury					
	3 mo		6 mo		12 mo		3 mo		6 mo		12 mo	
Grade	C	I	C	I	C	I	C	I	C	I	C	I
0	30	6	31	4	28	2	31	10	32	2	29	0
1	4	25	3	10	6	3	2	19	1	11	5	5
2	1	3	2	16	1	11	2	4	2	18	2	14
3	1	2	0	6	1	20	1	3	1	5	0	16

C = Control group; I = irradiation group.

Statistical analysis of data by rank sum test, compared with control group. Pathologic changes in irradiated area were significant, with all *P* values less than 0.05.

CONCLUSION

^{13}N-ammonia PET/CT MPI can detect irradiation-induced myocardial perfusion abnormalities together with global and regional left ventricular dysfunction at a very early stage of RIHD. Pathologic examination and coronary angiography suggest that the early myocardial perfusion abnormalities induced by irradiation are due to microvascular damage, myocardial degeneration, and interstitial fibrosis in the irradiated area rather than to coronary artery stenosis. ^{13}N-ammonia PET/CT MPI may be a valuable method for monitoring and evaluating RIHD, although its value in clinical practice will require further study for validation.

DISCLOSURE

This study was supported by grant 81171374 from the Natural Science Foundation of China. No other potential conflict of interest relevant to this article was reported.

ACKNOWLEDGMENTS

We thank Dr. Xiaoli Zhang for help and advice on the manuscript and the China Institute for Radiation Protection for technical support.

REFERENCES

1. Madan R, Benson R, Sharma DN, Julka PK, Rath GK. Radiation induced heart disease: pathogenesis, management and review literature. *J Egypt Natl Canc Inst.* 2015;27:187–193.
2. Chargari C, Riet F, Mazevet M, Morel E, Lepechoux C, Deutsch E. Complications of thoracic radiotherapy. *Presse Med.* 2013;42:e342–e351.
3. Yan R, Song J, Wu Z, et al. Detection of myocardial metabolic abnormalities by ^{18}F-FDG PET/CT and corresponding pathological changes in Beagles with local heart irradiation. *Korean J Radiol.* 2015;16:919–928.
4. Sridharan V, Tripathi P, Sharma S, et al. Roles of sensory nerves in the regulation of radiation-induced structural and functional changes in the heart. *Int J Radiat Oncol Biol Phys.* 2014;88:167–174.
5. Tillman GF, Pawlicki T, Koong AC, Goodman KA. Preoperative versus postoperative radiotherapy for locally advanced gastroesophageal junction and proximal gastric cancers: a comparison of normal tissue radiation doses. *Dis Esophagus.* 2008;21:437–444.
6. Weber DC, Peguret N, Dipasquale G, Cozzi L. Involved-node and involved-field volumetric modulated arc vs. fixed beam intensity-modulated radiotherapy for female patients with early-stage supra-diaphragmatic Hodgkin lymphoma: a comparative planning study. *Int J Radiat Oncol Biol Phys.* 2009;75:1578–1586.
7. Wu WC, Chan CL, Wong YW, Cuijpers JP. A study on the influence of breathing phases in intensity-modulated radiotherapy of lung tumours using four-dimensional CT. *Br J Radiol.* 2010;83:252–256.
8. Bhattacharya S, Asaithamby A. Ionizing radiation and heart risks. *Semin Cell Dev Biol.* 2016;58:14–25.
9. Darby SC, Ewertz M, McGale P, et al. Risk of ischemic heart disease in women after radiotherapy for breast cancer. *N Engl J Med.* 2013;368:987–998.
10. Davis M, Witteles RM. Radiation-induced heart disease: an under-recognized entity? *Curr Treat Options Cardiovasc Med.* 2014;16:317.
11. Zagar TM, Marks LB. Breast cancer: risk of heart disease after radiotherapy-cause for concern. *Nat Rev Clin Oncol.* 2013;10:310–312.
12. Varga Z, Cserhati A, Rarosi F, et al. Individualized positioning for maximum heart protection during breast irradiation. *Acta Oncol.* 2014;53:58–64.
13. Groarke JD, Nguyen PL, Nohria A, Ferrari R, Cheng S, Moslehi J. Cardiovascular complications of radiation therapy for thoracic malignancies: the role for non-invasive imaging for detection of cardiovascular disease. *Eur Heart J.* 2014;35:612–623.
14. Lancellotti P, Nkomo VT, Badano LP, et al. Expert consensus for multi-modality imaging evaluation of cardiovascular complications of radiotherapy in adults: a report from the European Association of Cardiovascular Imaging and the American Society of Echocardiography. *Eur Heart J Cardiovasc Imaging.* 2013;14:721–740.
15. Chargari C. The issue of radiation-induced cardiovascular toxicity: preclinical highlights and perspectives on preventive strategies. *Biomed J.* 2013;36:150–151.
16. Narain VS, Fischer L, Puri A, Sethi R, Dwivedi SK. Prognostic value of angiographic perfusion score (APS) following percutaneous interventions in acute coronary syndromes. *Indian Heart J.* 2013;65:1–6.
17. Tokatli F, Uzal C, Doganay L, et al. The potential cardioprotective effects of amifostine in irradiated rats. *Int J Radiat Oncol Biol Phys.* 2004;58:1228–1234.
18. Dogan I, Sezen O, Sonmez B, et al. Myocardial perfusion alterations observed months after radiotherapy are related to the cellular damage. *Nuklearmedizin.* 2010;49:209–215.
19. Azimzadeh O, Sievert W, Sarioglu H, et al. PPAR alpha: a novel radiation target in locally exposed *Mus musculus* heart revealed by quantitative proteomics. *J Proteome Res.* 2013;12:2700–2714.
20. Singh VP, Le B, Khode R, Baker KM, Kumar R. Intracellular angiotensin II production in diabetic rats is correlated with cardiomyocyte apoptosis, oxidative stress, and cardiac fibrosis. *Diabetes.* 2008;57:3297–3306.
21. Martinou M, Gaya A. Cardiac complications after radical radiotherapy. *Semin Oncol.* 2013;40:178–185.
22. Stewart FA, Seemann I, Hoving S, Russell NS. Understanding radiation-induced cardiovascular damage and strategies for intervention. *Clin Oncol (R Coll Radiol).* 2013;25:617–624.
23. Marks LB, Yu X, Prosnitz RG, et al. The incidence and functional consequences of RT-associated cardiac perfusion defects. *Int J Radiat Oncol Biol Phys.* 2005;63:214–223.
24. Prosnitz RG, Marks LB. Radiation-induced heart disease: vigilance is still required. *J Clin Oncol.* 2005;23:7391–7394.
25. Gayed IW, Liu HH, Yusuf SW, et al. The prevalence of myocardial ischemia after concurrent chemoradiation therapy as detected by gated myocardial perfusion imaging in patients with esophageal cancer. *J Nucl Med.* 2006;47:1756–1762.
26. Gayed IW, Liu HH, Wei X, et al. Patterns of cardiac perfusion abnormalities after chemoradiotherapy in patients with lung cancer. *J Thorac Oncol.* 2009;4:179–184.
27. Yu X, Prosnitz RR, Zhou S, et al. Symptomatic cardiac events following radiation therapy for left-sided breast cancer: possible association with radiation therapy-induced changes in regional perfusion. *Clin Breast Cancer.* 2003;4:193–197.
28. Sioka C, Exarchopoulos T, Tasiou I, et al. Myocardial perfusion imaging with ^{99m}Tc-tetrofosmin SPECT in breast cancer patients that received postoperative radiotherapy: a case-control study. *Radiat Oncol.* 2011;6:151.
29. Gyenes G, Fornander T, Carlens P, Glas U, Rutqvist LE. Detection of radiation-induced myocardial damage by technetium-99m sestamibi scintigraphy. *Eur J Nucl Med.* 1997;24:286–292.
30. Seddon B, Cook A, Gothard L, et al. Detection of defects in myocardial perfusion imaging in patients with early breast cancer treated with radiotherapy. *Radiother Oncol.* 2002;64:53–63.